

Actin polymerization as a key innate immune effector mechanism to control *Salmonella* infection

Si Ming Man^{a,1}, Andrew Ekpenyong^{b,c,1}, Panagiotis Tourlomis^a, Sarra Achouri^b, Eugenia Cammarota^b, Katherine Hughes^a, Alessandro Rizzo^a, Gilbert Ng^{b,c}, John A. Wright^a, Pietro Cicuta^b, Jochen R. Guck^{b,c}, and Clare E. Bryant^{a,2}

^aDepartment of Veterinary Medicine and ^bSector of Biological and Soft Systems, Cavendish Laboratory, University of Cambridge, Cambridge CB3 0ES, United Kingdom; and ^cBiotechnology Center, Technische Universität Dresden, 01307 Dresden, Germany

Edited by Vishva M. Dixit, Genentech, San Francisco, CA, and approved November 6, 2014 (received for review October 17, 2014)

Salmonellosis is one of the leading causes of food poisoning worldwide. Controlling bacterial burden is essential to surviving infection. Nucleotide-binding oligomerization domain-like receptors (NLRs), such as NLRC4, induce inflammasome effector functions and play a crucial role in controlling *Salmonella* infection. Inflammasome-dependent production of IL-1 β recruits additional immune cells to the site of infection, whereas inflammasome-mediated pyroptosis of macrophages releases bacteria for uptake by neutrophils. Neither of these functions is known to directly kill intracellular salmonellae within macrophages. The mechanism, therefore, governing how inflammasomes mediate intracellular bacterial-killing and clearance in host macrophages remains unknown. Here, we show that actin polymerization is required for NLRC4-dependent regulation of intracellular bacterial burden, inflammasome assembly, pyroptosis, and IL-1 β production. NLRC4-induced changes in actin polymerization are physically manifested as increased cellular stiffness, and leads to reduced bacterial uptake, production of antimicrobial molecules, and arrested cellular migration. These processes act in concert to limit bacterial replication in the cell and dissemination in tissues. We show, therefore, a functional link between innate immunity and actin turnover in macrophages that underpins a key host defense mechanism for the control of salmonellosis.

innate immunity | ASC | caspase-1 | cytoskeleton | ROS

A critical step in disease pathogenesis for many clinically important bacteria is their ability to infect and survive within host cells such as macrophages. *Salmonella enterica*, a pathogen that resides and replicates within macrophages, causes a range of life-threatening diseases in humans and animals, and accounts for 28 million cases of enteric fever worldwide each year (1). *S. enterica* infects phagocytes by a process that requires cytoskeletal reorganization (2). This bacterium resides in a *Salmonella*-containing vacuole (SCV) within host macrophages, and this intracellular lifestyle enables them to avoid extracellular antimicrobial killing, evade adaptive immune responses, and potentially to spread to new sites to seed new infectious foci within host tissue, which eventually develop into granulomas (3). Survival and growth of *S. enterica* within phagocytes is critical for virulence (4) and host restriction of the intracellular bacterial load is, therefore, paramount in surviving salmonellosis. *Salmonella* delivers microbial effector proteins into the host cell via the type III secretion systems (T3SS), mediated by the *Salmonella* pathogenicity island-1 and -2 (SPI-1 and SPI-2), to subvert cellular functions and facilitate intracellular survival (5).

Microbes are recognized by macrophages through pattern recognition receptors (PRRs), such as Toll-like receptors (TLRs) and nucleotide-binding oligomerization domain-like receptors (NLRs), which initiate innate immune responses, including cytokine production and pathogen killing (6). NLRs drive the formation of inflammasomes—macromolecular protein complexes—comprising one or more NLRs, usually an adaptor protein (ASC) and the effector protein caspase-1, which then cleaves

prointerleukin-1 β (IL-1 β) and pro-IL-18 into biologically active cytokines, and initiates macrophage cell death by pyroptosis (7). NLRC4, in concert with NAIPs 1, 2, 5, and 6, is a key PRR that forms an inflammasome complex upon sensing flagellin and/or the inner rod or needle proteins (PrgJ and PrgI, respectively) of the SPI-1 T3SS of *S. enterica* serovar Typhimurium (*S. Typhimurium*) (8–11). Activation of the NLRC4 inflammasome by *Salmonella* infection results in IL-1 β and IL-18 production driven by an ASC-dependent pathway and macrophage pyroptosis driven by an ASC-independent pathway (12, 13). A second, noncanonical, NLR signaling pathway has been described, which requires caspase-11 to initiate delayed cell death and NLRP3 inflammasome activation (14–16). Effective clearance of *Salmonella* infection in host cells may therefore require a coordinated effort between different inflammasome signaling pathways.

We, and others, have shown that NLRC4 is important in regulating bacterial burden of *S. Typhimurium* in vivo (17–19). A recent study revealed that *Salmonella*-infected epithelial cells are extruded from the intestinal epithelium in a process that requires NLRC4 (20). The molecular mechanism behind how NLRC4 restricts bacterial burden in macrophages infected with *Salmonella* is still unknown. Here, we identify an actin-dependent mechanism that controls NLRC4-mediated regulation of bacterial replication in macrophages infected with *S. Typhimurium*.

Significance

Infectious diseases are responsible for one-third of all mortality worldwide. Innate immunity is critical for mounting host defenses that eliminate pathogens. *Salmonella* is a global food-borne pathogen that infects and replicates within macrophages. How inflammasomes—multimeric protein complexes that provide innate immune protection—function to restrict bacterial burden in macrophages remains unknown. We show that actin polymerization is critical for NLRC4 inflammasome activation in response to *Salmonella* infection. NLRC4 activation in *Salmonella*-infected cells prevents further uptake of bacteria by inducing cellular stiffness and antimicrobial responses, which prevent bacterial dissemination in the host. These results demonstrate a critical link between innate immunity and the actin cytoskeleton in the cellular defense against *Salmonella* infection.

Author contributions: S.M.M., A.E., P.C., J.R.G., and C.E.B. designed research; S.M.M., A.E., P.T., S.A., E.C., K.H., A.R., G.N., and J.A.W. performed research; P.C. and J.R.G. contributed new reagents/analytic tools; S.M.M., A.E., P.T., S.A., E.C., K.H., P.C., J.R.G., and C.E.B. analyzed data; and S.M.M. and C.E.B. wrote the paper.

The authors declare no conflict of interest.

This article is a PNAS Direct Submission.

¹S.M.M. and A.E. contributed equally to this work.

²To whom correspondence should be addressed. Email: ceb27@cam.ac.uk.

This article contains supporting information online at www.pnas.org/lookup/suppl/doi:10.1073/pnas.1419925111/-DCSupplemental.

Activation of NLRC4 in infected macrophages mediates the production of reactive oxygen species (ROS) to inhibit bacterial replication and limits additional bacterial uptake by inducing mechanical stiffening the cell via actin polymerization. Overall, we describe a previously unidentified effector mechanism, governed by actin and the NLRC4 inflammasome, to control *Salmonella* infection in macrophages.

Results

The NLRC4 Inflammasome Controls Intracellular Bacterial Numbers in Macrophages. NLRC4 and NLRP3 inflammasomes are critical in controlling *Salmonella* infection in vivo (17–19); however, whether inflammasomes regulate intracellular bacterial load in macrophages is unknown. To investigate whether NLRC4 or NLRP3 regulate the burden of salmonellae in macrophages, we infected primary bone marrow-derived macrophages (BMMs) from WT, *Nlrc4*^{-/-}, *Nlrp3*^{-/-}, *Asc*^{-/-}, *Casp1*^{-/-}, or *Casp11*^{-/-} mice with a SPI-1-competent *S. Typhimurium* [multiplicity of infection (MOI) 1] and quantified the number of bacteria using gentamicin protection assays. After 2 h of infection, we found a significantly higher *Salmonella* burden in *Nlrc4*^{-/-} or *Casp1*^{-/-} BMMs compared with WT BMMs (Fig. 1A). The *Casp1*^{-/-} mouse strain was recently shown to be deficient in caspase-11 (herein referred to as *Casp1/11*^{-/-}) (14). *Casp1/11*^{-/-} BMMs infected with *S. Typhimurium*, however, contained similar number of bacteria compared with WT BMMs (Fig. S1), indicating that caspase-1, rather than caspase-11, controls bacterial numbers in macrophages at this time point. Confocal microscopy was performed on individual macrophages infected with a GFP-expressing strain of *S. Typhimurium* and the bacterial load per cell was enumerated. A higher number of bacteria per cell was found in *Nlrc4*^{-/-} and *Casp1/11*^{-/-} BMMs (most had 4–6 bacteria per cell) compared with WT cells (most had 1–2 bacteria per cell; Fig. 1B). These results indicate that the NLRC4–caspase-1 axis restricts bacterial numbers in macrophages.

We further confirmed these results by infecting WT BMMs with an isogenic mutant of *S. Typhimurium* lacking NLRC4 activators (Δ *fliC* Δ *fliB* (deletion of flagellin proteins) and Δ *prgJ*). We found that WT BMMs failed to restrict bacterial numbers in the absence of NLRC4 activation (Fig. 1C). Gentamicin protection assays and single-cell analysis of *Salmonella*-infected *Asc*^{-/-} or *Nlrp3*^{-/-} BMMs revealed similar total numbers and distribution of bacteria per cell compared with WT BMMs (Fig. 1A and B). Together, these results suggest that the NLRC4 inflammasome regulates *Salmonella* burden in macrophages via a mechanism that is independent of ASC.

NLRC4 Restricts Bacterial Replication in the *Salmonella*-Containing Vacuole. An elevated intracellular bacterial burden could occur by one or more of the following mechanisms: increased infection rate of macrophages, increased intracellular bacterial growth rate, or suppression of intracellular bacterial killing (21). When *S. Typhimurium* enters a macrophage, the cell must be able to limit bacterial replication to prevent overwhelming infection. The increased number of bacteria per cell in *Nlrc4*^{-/-} BMMs suggests a role for NLRC4 in the inhibition of intracellular bacterial survival (Fig. 1). *S. Typhimurium* survive and replicate intracellularly in macrophages within SCVs of a diameter of 3–4 μ m (Fig. S2). We used live confocal imaging to record the number of bacteria in each SCV over time and calculated the bacterial growth rate within each SCV from WT ($n = 11$) and *Nlrc4*^{-/-} ($n = 30$) BMMs over 17 h. In WT BMMs that were not killed by pyroptosis, the bacterial growth rate in the SCV was 0.12 divisions per hour. Bacteria in the SCVs of *Nlrc4*^{-/-} BMMs, in contrast, grew twice as fast—at a rate of 0.24 divisions per hour (Fig. 2A). These results indicate that *Nlrc4*^{-/-} BMMs fail to effectively restrict bacterial replication in the SCV. Effective

control of intracellular *Salmonella* by macrophages has been shown to be mediated by mitochondrial ROS (mROS) activity and hydrogen peroxide produced within the cell (22). We measured mROS activity and cellular hydrogen peroxide production in BMMs infected with *S. Typhimurium* for 30 min and found that WT BMMs generated mROS activity and hydrogen peroxide after infection with *S. Typhimurium*, whereas *Nlrc4*^{-/-} or *Casp1/11*^{-/-} BMMs failed to induce mROS or hydrogen peroxide (Fig. 2B and C). *Nlrp3*^{-/-} BMMs produced mROS and hydrogen peroxide at a level comparable to WT BMMs (Fig. 2B and C), indicating that NLRC4, but not NLRP3, induces ROS in macrophages in response to *Salmonella* infection. Furthermore, inhibition of ROS in BMMs with *N*-acetyl-L-cysteine (NAC) resulted in a significantly increased number of intracellular

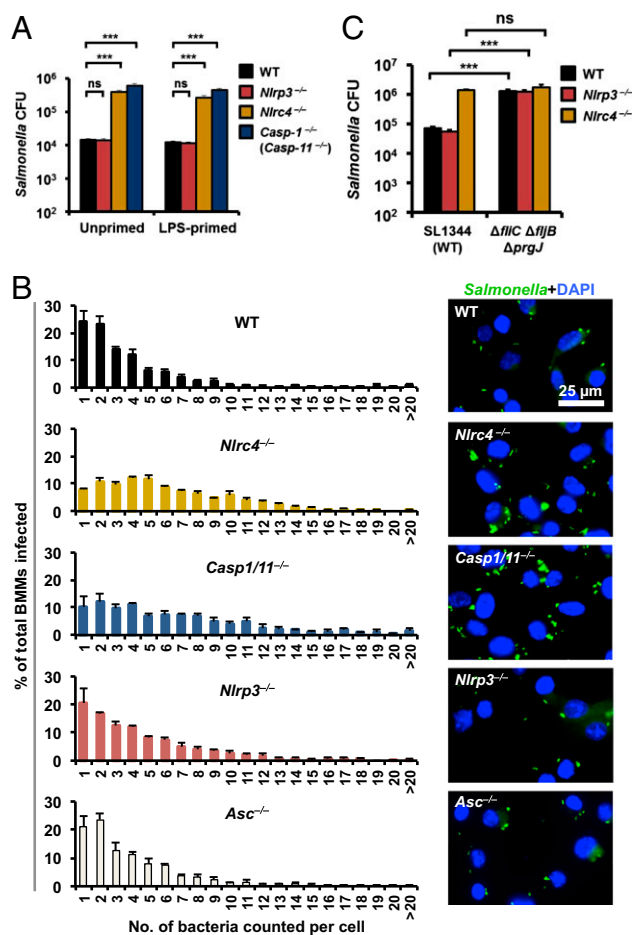


Fig. 1. The NLRC4–caspase-1 axis restricts high levels of intracellular *S. Typhimurium* numbers in macrophages. (A) Unprimed primary BMMs were infected with *S. Typhimurium* (MOI 1) for 1 h. Following 1-h infection, BMMs were treated with gentamicin (50 μ g/mL) for 1 h to kill extracellular bacteria. Host cell lysates were plated onto LB agar and the number of viable intracellular bacteria was enumerated. (B) Unprimed BMMs were infected with *S. Typhimurium* expressing GFP (MOI 10) for 1 h, followed by gentamicin treatment (50 μ g/mL) for 1 h to kill extracellular bacteria. The percentages of BMMs harboring different number of bacteria were determined by microscopy (WT, $n = 1,134$; *Nlrc4*^{-/-}, $n = 765$; *Casp1/11*^{-/-}, $n = 708$; *Nlrp3*^{-/-}, $n = 663$; *Asc*^{-/-}, $n = 731$). (C) Unprimed BMMs were infected with Δ *fliC* Δ *fliB* Δ *prgJ* *S. Typhimurium* (MOI 1) for 1 h and the number of viable intracellular bacteria was enumerated. Data are the mean of three independent experiments and error bars represent SEM. (A) One-way ANOVA with a Dunnett's multiple comparisons test. (C) Two-way ANOVA with a Tukey's multiple comparisons test. *** $P < 0.001$; ns, no statistical significance.

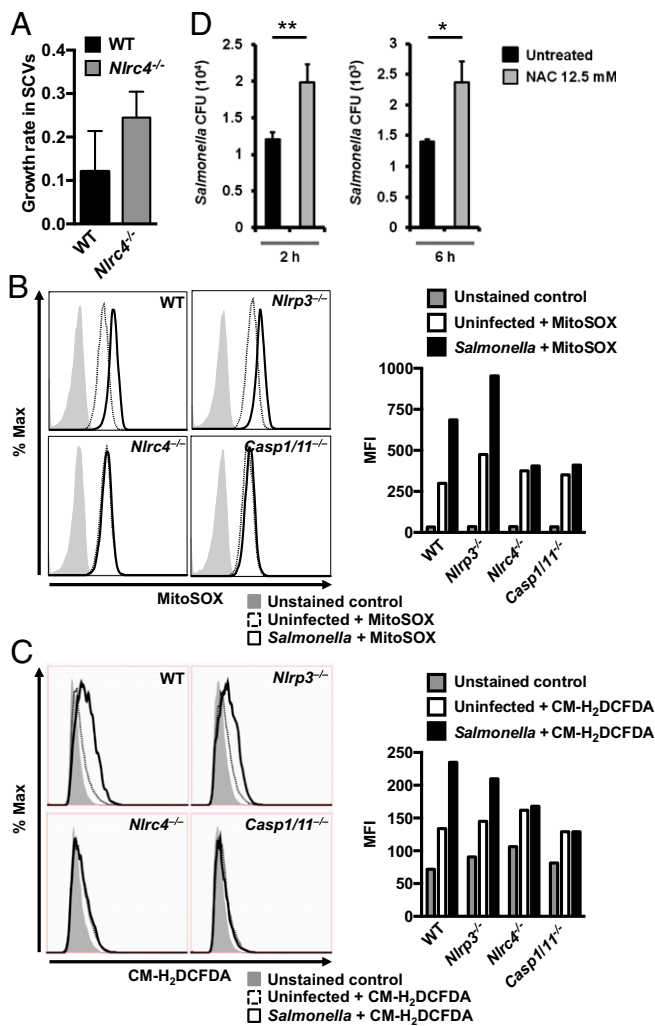


Fig. 2. NLRC4 regulates mitochondrial ROS and H_2O_2 production to restrict bacterial replication by *Salmonella* in the SCV. (A) The bacterial growth rate in each SCV was determined in WT and *Nlrc4*^{-/-} BMMs using live confocal imaging of SCVs (WT, $n = 11$; *Nlrc4*^{-/-}, $n = 30$) over 17 h following inoculation. The growth rate of *S. Typhimurium* was calculated using the formula $\Delta n/t$, where Δn is the number of bacteria in a SCV immediately before the death of a macrophage minus the number of bacteria following the formation of a SCV, and t is the length of time that the macrophage had survived over the course of the infection. (B and C) Unprimed BMMs were infected with *S. Typhimurium* (MOI 10) for 30 min and stained with MitoSOX stain or CM- H_2 DCFDA for 30 min. (B) Levels of mROS and (C) H_2O_2 were measured using flow cytometry. (D) WT BMMs were treated with NAC for 1.5 h and then infected with *S. Typhimurium* (MOI 1) for 1 h, followed by gentamicin treatment for a total of 2 or 6 h. Lysates from BMMs were plated on LB agar and the number of viable intracellular bacteria was enumerated. Data are representative of three (C and D) or four (B) independent experiments. Error bars indicate SEM. Two-tailed t test, * $P < 0.05$; ** $P < 0.01$.

bacteria compared with untreated controls following 2 and 6 h of infection ($P = 0.007$ for 2 h and $P = 0.013$ for 6 h; Fig. 2D). These results collectively demonstrate that NLRC4 contributes to the restriction of bacterial replication in SCVs.

NLRC4 Modifies Actin Polymerization to Activate Inflammasome Responses to *Salmonella* Infection. Our live-cell imaging experiments using confocal microscopy revealed important differences in the growth rate of bacteria in WT and *Nlrc4*^{-/-} macrophages. To further investigate the dynamics of the infection process, we used live-cell imaging to track and quantify infection events

of individual WT and *Nlrc4*^{-/-} macrophages infected with *S. Typhimurium*-GFP (MOI of 10) every 60 s for 1 h. WT BMMs were susceptible to infection for the first 10 min, but susceptibility to infection plateaued after 10 min, whereas *Nlrc4*^{-/-} BMMs were initially less susceptible to infection compared with WT BMMs (0–30 min), but remained readily susceptible to infection over time (Fig. 3A). The failure to limit bacterial uptake in the absence of NLRC4 ultimately resulted in a greater number of total infection events per macrophage after 1 h of infection (6.8 ± 1.0 bacteria per *Nlrc4*^{-/-} BMMs vs. 5.0 ± 0.7 bacteria per WT BMMs).

Cytoskeletal rearrangement, particularly changes in actin conformation, is an important process for entry of *Salmonella* into epithelial cells (23); however, it is unknown whether NLRC4 regulates cytoskeletal function to control infection in macrophages. We hypothesized that NLRC4 might alter cytoskeletal function to reduce bacterial uptake in macrophages. Inhibition of host cell actin polymerization and reduced actin availability, using cytochalasin D (24, 25), significantly impaired *Salmonella* uptake into macrophages, whereas colchicine (a microtubule polymerization inhibitor) failed to significantly inhibit bacterial

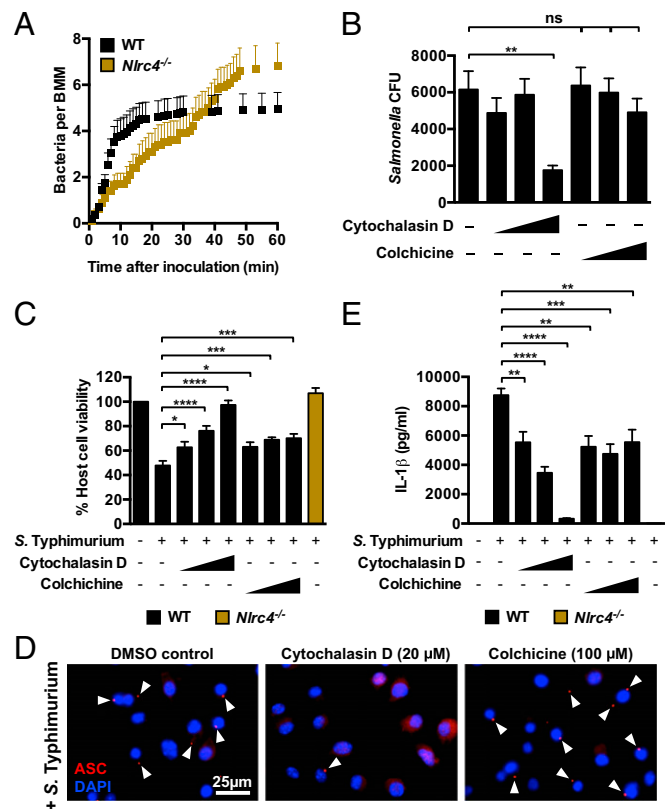


Fig. 3. NLRC4 inflammasome functions are linked to the actin cytoskeleton. (A) Unprimed BMMs were infected with *S. Typhimurium* expressing GFP (MOI 10) and tracked by confocal live imaging for 1 h. The number of bacteria internalized into each macrophage was counted every 60 s. (B) The number of viable intracellular bacteria recovered from WT BMMs infected with *S. Typhimurium* in the presence of the vehicle control DMSO, cytochalasin D (0.2, 2, and 20 μ M) or colchicine (1, 10, and 100 μ M) was counted. (C) Host cell viability and (D) levels of IL-1 β secreted from LPS-primed WT BMMs infected with *S. Typhimurium* for 1 h in the presence of the vehicle control DMSO, cytochalasin D, or colchicine. (E) Unprimed WT BMMs were infected with *S. Typhimurium* for 1 h and stained for ASC (red) and DNA (blue). Data are the mean of three independent experiments and error bars represent SEM. One-way ANOVA with a Dunnett's multiple comparisons test. * $P < 0.05$; *** $P < 0.001$; **** $P < 0.0001$; ns, not statistically significant.

uptake after 2 h of infection (Fig. 3B). Cytochalasin D also dose-dependently inhibited *Salmonella*-induced NLRC4-dependent pyroptosis (Fig. 3C).

NLRC4 is unusual among the inflammasome-forming NLRs in that it can activate caspase-1 directly by CARD–CARD domain interactions as well as through association with the adaptor protein ASC (26, 27). Our data suggest that changes in actin polymerization are an important effector mechanism for NLRC4-dependent ASC-independent antimicrobial effects induced by the cell, and we wondered whether this would also be true for ASC-dependent NLRC4 inflammasome activation by *S. Typhimurium*. Inflammasome activation drives the formation of a large macromolecular complex, or “speck,” within the cell whereby ASC forms the platform for recruitment of effector proteins in response to *Salmonella* infection (17, 28). We infected BMMs with *S. Typhimurium* and immunolocalized ASC at different time-points and observed the formation of an ASC speck within 5 min postinfection (Fig. S3). The formation of macromolecular protein complexes can be facilitated by cytoskeletal reorganization. We found that cytochalasin D, but not colchicine, inhibited the formation of these rapidly induced ASC inflammasome specks in *Salmonella*-infected BMMs (Fig. 3D). ASC speck formation is critical for the production of IL-1 β , and in our experiments cytochalasin D indeed dose-dependently blocked early NLRC4-dependent *Salmonella*-induced IL-1 β production, whereas colchicine did not dose-dependently inhibit *Salmonella*-induced IL-1 β production (Fig. 3E). We further confirmed these results and found that cytochalasin D, but not colchicine, inhibited flagellin-induced ASC speck formation and IL-1 β secretion in BMMs (Fig. S4). These results suggest that actin polymerization provides a mechanism by which NLRC4 activates innate immunity in response to *S. Typhimurium*.

Activation of NLRC4 Modulates Macrophage Deformability and Movement. We hypothesized that NLRC4-dependent changes in actin polymerization should impact cytoskeletal functions within the cell; to investigate this, we used an optical stretcher, an established biophysical instrument (29), to determine whether there is a dynamic change in the cytoskeletal function of WT and *Nlrc4*^{-/-} BMMs in response to *Salmonella* infection. The optical stretcher employs two counterpropagating laser beams to trap and deform individual macrophages and measure changes in their deformability or compliance (the inverse of stiffness), which is dependent on the functionality of the cytoskeleton (Fig. 4A) (30). When coupled to a fluorescence detector, it is possible to trap and specifically stretch cells that had been infected with GFP-expressing *S. Typhimurium*. We analyzed uninfected WT or *Nlrc4*^{-/-} BMMs or BMMs infected with *S. Typhimurium*-GFP at an MOI of 10 for 10 min using the optical stretcher. The BMMs were trapped and stretched for 4 s, followed by quantification of their compliance. We found that uninfected WT or *Nlrc4*^{-/-} BMMs exhibited identical viscoelastic properties. Infected WT BMMs, however, exhibited a change in their viscoelastic properties, such that the macrophages became less deformable or stiffer compared with uninfected WT cells (Fig. 4B). Remarkably, *Nlrc4*^{-/-} BMMs infected with *S. Typhimurium* showed little change in cell compliance, indicating that infection-induced cell stiffening did not occur (Fig. 4B).

We further confirmed the impact of NLRC4 on actin functionality with the use of phalloidin staining and 3D microscopy to reconstruct the F-actin cytoskeleton to visualize actin reorganization in response to *Salmonella* infection. In WT immortalized BMMs infected with a strain of *S. Typhimurium* expressing GFP at an MOI of 10, F-actin formed a dense network, indicated by the intense red staining around the bacterium at 5 min postinfection (Fig. 4C). *Nlrc4*^{-/-} immortalized BMMs infected with *S. Typhimurium* showed diffused actin staining

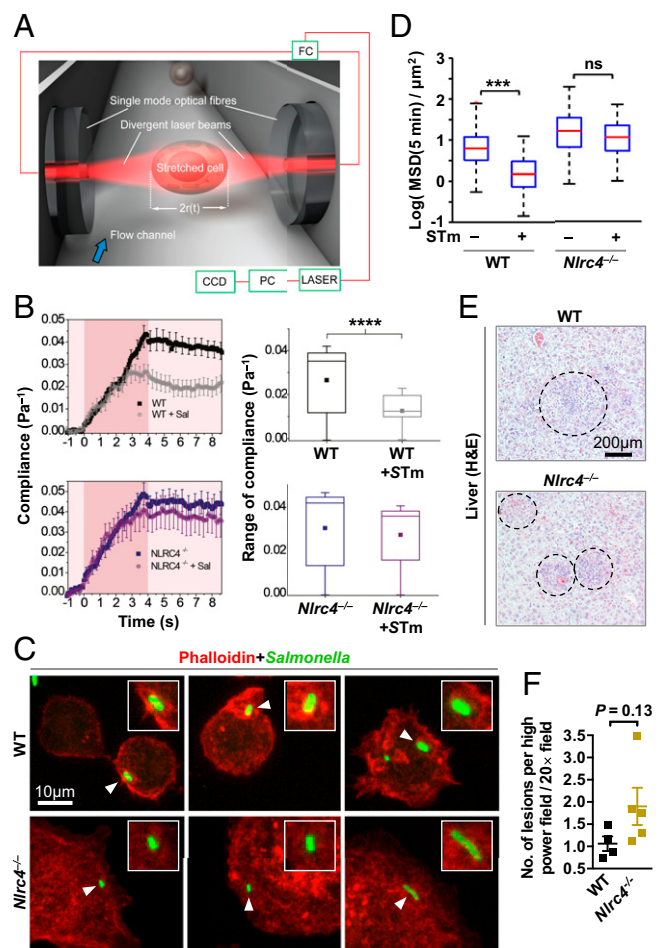


Fig. 4. NLRC4 activation induces physical stiffening of macrophages by limiting actin availability for bacterial uptake and impairs bacterial dissemination. (A) The principle and setup of the optical stretcher. Two diverging and counterpropagating laser beams emanating from single-mode optical fibers are used to trap and deform single suspended cells. A 50:50 intensity-ratio fiber coupler (FC) is used to split the output of a fiber laser into the two optical fibers. A personal computer (PC) is used for laser control and data acquisition by video microscopy via a CCD camera. (B) Unprimed primary BMMs were infected with GFP-expressing *S. Typhimurium* (MOI 10) for 10 min. BMMs were then serially trapped and stretched outwardly along the laser beam axis. Shown are (Left) the average creep compliance responses of the various cells during the 4 seconds of stretching (indicated by darker red) and (Right) box plots of the average compliance during the stretch. (C) A 3D reconstruction of phalloidin-stained F-actin cytoskeleton (red) in unprimed immortalized BMMs infected with GFP-expressing *S. Typhimurium* (MOI of 10) for 5 min. (D) Unprimed primary BMMs were imaged for 3 h and then infected with *S. Typhimurium* (MOI 10) and imaged for 30 min. For each cell, the movies were divided in sections of 10 min and cell movement was analyzed. Data shown are from uninfected cells (over the 3-h time period) and from cells infected with *S. Typhimurium* for 20–30 min. The mean square displacement (MSD) ($\text{MSD}(\tau) = \langle (x(t+\tau) - x(t))^2 \rangle_t$) of infected cells compared with uninfected cells ($\tau = 2\text{--}10$ min) is fitted with a power law $D_{\text{eff}} \cdot t^\alpha$. From the resulting fit, the value of the MSD at 5 min is calculated. In the box plot, the red bars represent the median of the distribution, the blue edges of the box indicate the 25th and 75th percentile, and dashed bars indicate the extreme points. (E) Histopathology of livers from WT ($n = 4$) and *Nlrc4*^{-/-} ($n = 5$) mice i.v. infected with *S. Typhimurium* for 7 d. Dashed circles indicate extent of lesions. (F) Livers were fixed and lesions were counted from four liver sections from each mouse. Two-tailed *t* test, *** $P < 0.001$; **** $P < 0.0001$; ns, not statistically significant.

proximal to the bacteria, which failed to form a striking stranded pattern observed in WT cells (Fig. 4C). This process could result in a localized “stiff” region to limit the size of the SCV and may restrict bacterial growth.

A consequence of cytoskeletal rearrangements that lead to increased cell stiffness can be impaired cellular movement (31). To investigate whether *Salmonella*-induced cellular stiffness mediated by NLRC4 affects macrophage migration, we tracked the movement of uninfected primary WT and *Nlrc4*^{-/-} BMMs for 3 h before infection and for the first 30 min postinfection. Both WT and *Nlrc4*^{-/-} BMMs moved freely before infection (Fig. 4D, Fig. S5, and Movie S1). Following infection with *S. Typhimurium*, the movement of WT BMMs ceased rapidly, whereas the movement of *Nlrc4*^{-/-} BMMs was unaffected, despite the increasing intracellular bacterial burden (Fig. 4D and Movie S1). Our data therefore suggest that *Salmonella* infection activates the NLRC4 inflammasome to cause major cytoskeletal reorganization in macrophages, reducing macrophage movement, and susceptibility to infection. To confirm the physiological relevance of cellular movement in the control of salmonellosis, we performed histological analysis of liver tissue sections to investigate the number of infectious foci (lesions or granulomas induced by *Salmonella* and macrophage recruitment (3)) from mice infected with *S. Typhimurium*. An increase in bacterial burden is associated with an increase in lesion number (3). We saw an increase in bacterial burden and the number of infectious foci in *Nlrc4*^{-/-} mice compared with WT mice (Fig. 4E and F and Fig. S6). Taken together, our results suggest that NLRC4 activation by *Salmonella* infection changes cytoskeletal dynamics and leads to important physiological functions, including reduced cellular movement, suppression of bacterial uptake, and production of antimicrobial molecules, which together leads to a reduced intracellular bacterial burden that can be effectively cleared by the cell.

Discussion

Inflammasome activation provides host protection against infectious agents. The NLRC4 inflammasome is activated in response to *Salmonella* infection, inducing caspase-1-dependent cleavage and release of bioactive IL-1 β and IL-18 and pyroptosis. Pyroptosis of macrophages leads to release of bacteria for uptake by other cell types, such as neutrophils, but also permits bacterial dissemination (18). Neutrophils, for example, do not undergo NLRC4-mediated pyroptosis and provide a major source of IL-1 β during *Salmonella* infection (32), which indicates that pyroptosis is not always required for the control of pathogen burden. Here, we have shown that macrophages that resist pyroptosis can directly control and restrict intracellular salmonellae. *Salmonella*-induced NLRC4 inflammasome activation is intimately linked to actin polymerization, where F-actin filaments are recruited to the bacteria within 5 min of infection. Efficient reorganization of the actin cytoskeleton is required for rapid ASC speck formation, a hallmark of inflammasome assembly (17, 28), which occurs within 5 min of infection.

Mechanical correlates of actin reorganization can be measured using an optical stretcher, which determines the dynamic change of the cytoskeleton and changes in its compliance. We found that *Salmonella* infection and activation of the NLRC4 inflammasome induces cellular stiffness in macrophages such that the cell has an impaired ability to take up more bacteria. This finding raises the question of whether limiting the uptake of bacteria in a cell is of benefit to the host.

Host macrophages infected by *Salmonella* may direct their resources to killing the residing bacteria before uptake of more bacteria. This strategy may avoid overwhelming infection, thereby allowing more effective clearance of a small number of intracellular bacteria at a time and to avoid pyroptosis. Importantly, we found that activation of the NLRC4 inflammasome is required for generating ROS and restrict intracellular bacterial replication in the SCV.

Bacterial uptake concomitantly induces cell stiffness and impairs cellular movement. The use of actin to target and surround the invading bacteria may also reduce the total amount of actin available for cellular movement, which reduces macrophage migration and dissemination of infected cells to other areas of the

tissue. Indeed, mice lacking NLRC4 exhibit increased numbers of infectious foci in liver tissues and are more susceptible to salmonellosis. A previous study has identified that β -actin and γ -actin are targets for caspase-1 cleavage (33). It is possible that *Salmonella*-induced NLRC4 inflammasome activation drives cleavage and modification of actin to arrest cellular movement. Inflammasome-induced cellular stiffening and arrest may represent a general mechanism for the control of intracellular bacterial infection. Earlier work showed that CD4⁺ T lymphocytes infected with *Shigella flexneri* exhibit an impaired ability to migrate in vitro and in vivo (34, 35). *Shigella* can drive inflammasome activation through both NLRC4 and NLRP3 (36, 37), but it remains to be determined whether increased cell stiffness and impaired movement in immune cells are a consequence of inflammasome activity induced by pathogens other than *Salmonella*, such as *Shigella* or *Listeria*. In conclusion, our work has identified a key cellular mechanism driven by the NLRC4 inflammasome and actin polymerization to reduce intracellular *Salmonella* burden in macrophages. The fate of a macrophage and the bacterium, therefore, depends on the host-microbial engagement of the NLRC4 inflammasome, which is governed by the number of bacteria that infect and are taken up by the cell, and the ability of the bacteria to replicate or resist bacterial killing.

Materials and Methods

Bacterial Strains. *S. Typhimurium* strain SL1344 and *S. Typhimurium* SL1344 Δ *fliC* Δ *fliB* Δ *prgJ* and the GFP-expressing strain JH3016 were used and described previously (17, 38).

Fluorescence and Confocal Microscopy and Analysis. To investigate the number of bacteria per macrophage, primary BMMs were infected with *S. Typhimurium* JH3016 (38), a derivative of SL1344 that expresses GFP, for 1 h, followed by gentamicin treatment (50 μ g/mL) for 1 h to kill extracellular bacteria. BMMs were washed twice with PBS and fixed in 4% (wt/vol) paraformaldehyde for 15 min. Cells were counterstained in DAPI mounting medium (Vector Labs). The number of bacteria per infected BMM was counted, and at least 200 infected BMMs of each genotype were counted in each of the three independent experiments.

To visualize the formation of the ASC speck in primary BMMs, cells were infected with *S. Typhimurium* strain SL1344 for 5, 10, and 20 min. BMMs were washed twice with PBS and fixed in 4% (wt/vol) paraformaldehyde for 15 min. Blocking was performed using 10% (vol/vol) normal goat serum (Dako) in 0.1% saponin (wt/vol; Sigma) for 1 h. Cells were stained with a rabbit anti-ASC antibody (1:500 dilution, AL177, AG-25B-0006-C100; Adipogen) for 40 min followed by Alexa Fluor 568 anti-rabbit (1:250 dilution; Life Technologies) for 50 min. Cells were counterstained in DAPI mounting medium (Vector Labs). Cells were visualized and imaged using a Leica DM6000 B fluorescence microscope.

For phalloidin staining and 3D reconstruction, immortalized BMMs were detached using Accutase solution (Sigma) and seeded onto glass-bottomed well chambers in serum limiting DMEM for 4 h. Supernatant was aspirated and *S. Typhimurium* JH3016 (MOI 10) was added. After 5 min, samples were aspirated and washed with PBS, fixed with 4% (wt/vol) paraformaldehyde for 10 min, blocked with 5% (wt/vol) BSA for 60 min, and stained with anti-*Salmonella* O antigen antibody (1:1,000 dilution, R30956901, Remel, Thermo Scientific) for 60 min. Samples were washed with PBS and stained with Alexa Fluor 488 anti-rabbit IgG (1:1,000 dilution; Life Technologies) and phalloidin-568 (1:50 dilution; Life Technologies) for 60 min. Samples were washed with PBS three times and mounted with DAPI mounting medium (Vector Labs). Samples were imaged on the Leica SP5 laser scanning confocal microscope (63 \times , 1.4 N.A.) and analyzed using LAS AF software (Leica).

Optical Stretcher. We used a microfluidic optical stretcher—a specific dual-beam optical trap capable of inducing well-defined stresses on whole single cells in suspension—to measure the overall deformability and creep compliance of cells (29, 30, 39).

All work involving live animals complied with the University of Cambridge Ethics Committee regulations and was performed under the Home Office Project License number 80/2572. Detailed information is presented in [SI Materials and Methods](#).

ACKNOWLEDGMENTS. We thank K. A. Fitzgerald (University of Massachusetts Medical School) and E. Creagh (Trinity College) for supplying the knockout mouse strains. Financial support for this work was provided by a Cambridge

Supporting Information

Man et al. 10.1073/pnas.1419925111

SI Materials and Methods

Mice. WT C57BL/6 mice were from Harlan. *Nlrc4*^{-/-}, *Nlrp3*^{-/-}, *Asc*^{-/-}, *Casp1/11*^{-/-} (Millennium Pharmaceuticals), and *Casp11*^{-/-} mice (E. Creagh, Trinity College, Dublin) were housed in a specific pathogen-free facility and all procedures carried out in accordance with the Animals Scientific Procedures Act 1986 outlined by UK Home Office regulations.

Cell Culture, Inflammasome Activators, and Inhibitors. Primary BMMs were generated by cultivating mouse bone marrow in BMM media consisting of DMEM (Sigma), 10% (vol/vol) heat-inactivated FCS (HyClone; Thermo Fisher Scientific), 5 mM L-glutamine (Sigma), 20% (vol/vol) L929 conditioned media, and 10 µg/mL gentamicin (Sigma) on Petri dishes for 6 d. RAW 264.7 macrophages and immortalized WT and *Nlrc4*^{-/-} BMMs were cultured in DMEM supplemented with 10% (vol/vol) FCS. For LPS priming, BMMs were stimulated with 200 ng/mL of ultrapure LPS from *Escherichia coli* (InvivoGen) for 3 h. WT *S. Typhimurium* strain SL1344 and *S. Typhimurium* SL1344 Δ *fliC* Δ *fliB* Δ *prgJ* were used (1). Ultrapure flagellin (60 ng) from *S. Typhimurium* (InvivoGen) was transfected into BMMs using Profect-P1 reagent (Targeting Systems). Flagellin and Profect-P1 were mixed and incubated for 20 min at room temperature, added to BMMs (in 40-mL volume per well in a 96-well plate) and centrifuged at 11 × *g* for 10 min. For inhibitor experiments, BMMs were incubated with 0.2, 2, or 20 µM cytochalasin D (Sigma) or 1, 10, or 100 µM colchicine (Sigma) at the same time as bacterial infection or ligand stimulation. To inhibit ROS, BMMs were pretreated with 12.5 mM NAC (Sigma) for 1 h. Inhibitors were used continuously throughout the experiment.

Gentamicin Protection Assay. BMMs were seeded onto 96-well plates at 2 × 10⁵ cells per well in antibiotic-free media and incubated overnight. WT *S. Typhimurium* strain SL1344 and *S. Typhimurium* SL1344 Δ *fliC* Δ *fliB* Δ *prgJ* were used. Bacteria were inoculated into LB broth and incubated for 17.5 h at 37 °C with agitation at 200 rpm, then subcultured (1:10) into fresh LB broth and incubated for a further 2 h. *S. Typhimurium* was then diluted in antibiotic-free BMM media to the indicated MOIs and added into wells containing BMMs. When bacterial mutants were used, bacteria were centrifuged onto BMMs at 500 × *g* for 10 min. Bacteria resuspended in BMM media were plated onto LB agar plates to confirm the number of viable bacteria added per well. For 2-h infections, bacteria was removed after 1 h and replaced with media containing 50 µg/mL gentamicin (Sigma) for 1 h to kill extracellular bacteria. For 6- and 24-h infections after 1-h incubation in media containing 50 µg/mL gentamicin, supernatant was removed and replaced with media containing 10 µg/mL gentamicin. BMMs were washed twice with antibiotic-free media and lysed in 0.5% (vol/vol) Triton X-100 for 20 min at 4 °C. Host cell viability was determined using the CytoTox 96 Non-Radioactive Cytotoxicity Assay (Promega). To determine the number of intracellular bacteria, 10-fold dilutions of the cell lysate were plated onto LB agar. The cfu grown on LB agar were enumerated following overnight incubation at 37 °C.

Live Imaging and Image Analysis. To determine the rate of bacterial uptake, unprimed WT and *Nlrc4*^{-/-} BMMs were infected with *S. Typhimurium* JH3016 at an MOI of 10 and tracked for 1 h using confocal live imaging. The number of bacteria internalized into each macrophage was counted every 60 s. To calculate the bacterial growth rate in each SCV, WT and *Nlrc4*^{-/-} BMDMs

were infected with *S. Typhimurium* JH3016 for 15 min. Gentamicin was then added (10 µg/mL) and images were acquired over 17 h. For each macrophage, the increase in the number of internalized bacteria, represented by Δn , was calculated by the number of bacteria in a SCV immediately before the death of a macrophage minus the number of bacteria immediately following the formation of a SCV. We also determined the survival time of the same infected macrophage following infection (*t*). For macrophages that had survived for the entire 17-h recording, 17 h was used as *t*. The bacterial growth rate was determined by the formula $\Delta n/t$. For measurement of the diameter of SCVs, RAW 264.7 macrophages were infected with *S. Typhimurium* strain SL1344 and imaged for 30 min with a time lapse of 754 ms using confocal microscopy. The diameter of each SCV was measured using the scale bar tool of the LASAF Lite software. Measurements were taken once the SCVs reached a stable size (no further change in size following formation for the rest of the experiment). Thirty-nine SCVs were measured over three separate experiments. All living imaging was acquired with a Leica SP5 confocal microscope using a 40× 1.25 N.A.

Optical Stretcher. We used a microfluidic optical stretcher (OS), which is a specific dual-beam optical trap capable of inducing well-defined stresses on whole single cells in suspension, to measure the overall deformability and creep compliance of cells (2–4). Details of the OS in terms of principle, setup, and routine handling have been previously described (2, 5). A personal computer is used for laser control and data acquisition done by video microscopy via a CCD camera (ORCA-05 G; Hamamatsu). In this work, the OS setup was placed on an inverted microscope (Eclipse TE2000-U; Nikon). The objective used was a 40× air objective (Plan Fluor ELWD/0.60 N.A., Ph2 LDL; Nikon); it was combined with a 1.5× auxiliary objective lens to give 60× resultant magnification. A broad-spectrum mercury discharge lamp provided illumination for fluorescence microscopy. The laser source was a single-mode, continuous-wave laser (YLM-5-1070-LP; IPG Photonics) operating at the near-infrared wavelength of 1,064 nm. The waveform of the fiber laser was coupled into two optical fibers using a 50:50 intensity-ratio fiber coupler (FC 1064 Single Mode Coupler; Thorlabs). Cells were introduced into a microfluidic delivery system, serially trapped, and then stretched outwardly along the laser beam axis (Fig. 4A). The forces that trap and deform the cell arise from the change in the refractive index (RI) at the cell–medium interface and the ensuing conservation of momentum (5). The elongation of the cell along the laser beam axis is recorded by the CCD camera. The axial strain during optical stretching is given by

$$\epsilon(t) = \frac{r(t)}{r_0} - 1,$$

where r_0 is the semimajor axis of the nonstretched cell and $r(t)$ is the time-varying semimajor axis measured. The optical stress on the cells is computed using an electromagnetic wave model (6, 7), which requires knowledge of the average RI of cells. We measured the average RI of BMMs (WT, *Nlrc4*^{-/-}, and *Casp1/11*^{-/-}, both infected and uninfected) using a digital holographic microscope (8). Thus, the mechanical properties of BMMs reported here are decoupled from their optical characteristics (9).

The strain for each cell is normalized by the peak value of the calculated optical stress σ_0 and a geometric factor F_g to give the time-dependent compliance,

$$J(t) = \frac{\epsilon(t)}{\sigma_0 F_g}$$

The geometric factor, calculated as described elsewhere (10), accounts for cell shape and stress distribution. Compliance data are presented as mean \pm SEM.

Cell Movement Analysis. Primary BMMs were plated on a 35-mm glass-bottom dish at a concentration of 2×10^6 cells in antibiotic-free culture medium for 8 h at 37 °C and 5% CO₂. The dish was mounted on the stage of a microscope for live-cell imaging and kept at 37 °C and 5% CO₂ during the experiment in a climate chamber. Live-cell imaging was performed with Leica TCS SP5 confocal microscope. Images were sequentially taken on a 40 \times oil-immersion objective with a 1.2 \times camera zoom every 7 s for 3 h before infection and 30 min postinfection with *S. Typhimurium* JH3016 (MOI 10). The image dimension used was 512 \times 512 pixels. The pinhole size was 1 a.u., and the thickness of the focal plane was 0.96 μ m. GFP was excited by an argon laser at 488 nm with 15% laser power. Acquired images were exported as 16-bit TIFF files for analysis. A custom-built MatLab script was used to automatically segment and track the cells.

Different criteria are used to separate the cell from the background as shown in Fig. S5. High- and low-intensity regions (Fig. S5 A–C) are defined through thresholds. The thresholds are set as $(m + p1 \times \sigma)$ and $(m - p2 \times \sigma)$, where m and σ are the mean and SD of the background intensity distribution, and $p1$ and $p2$ parameters that are adjusted manually for each movie and depend on the contrast. Another criterion is the intensity gradient (Fig. S5 D and E) defined as the sum of the squares of the intensity differences of neighbor pixels along row and columns in the image; it is also used as a spatial SD filter (Fig. S5 F and G) with a window of 3 \times 3 pixels and temporal SD (Fig. S5 H and I) on five consecutive frames. In all of the cases, the high level thresholds are set manually checking the output quality. The discriminated regions are superimposed (Fig. S5J), and then the area of interest is isolated according to its size and position. The final mask (Fig. S5 K and L) is then obtained applying morphological operations of holes filling, dilation, and erosion; the frames in which it is visible a mismatch between the segmented area and the cell area are removed. At each time point, the position of the cell is taken as the centroid of the segmented region. Bacteria were tracked from images taken using the GFP channel. Infected and noninfected cells were discriminated on the basis of the presence or absence of bacteria within the area occupied by the cell. For each cell, the mean square displacement from 2 to 10 min is fitted with a power law $D_{eff} \cdot t^\alpha$.

In Vivo Analyses of Bacterial Numbers and Lesion Formation. The 6- to 8-wk-old mice were i.v. infected with *S. Typhimurium* strain

M525P grown overnight at 37 °C in static culture in LB medium. Bacteria resuspended in PBS were injected into the tail veins of mice, and after 7 d killed by cervical dislocation. Spleens and livers were homogenized in a Colworth stomacher, and the number of viable bacteria was determined by plating on LB agar. For histological analysis of liver lesions, liver tissue was collected, fixed in paraformaldehyde, and embedded in paraffin. Liver sections were generated ($n = 4$ per liver), and lesions in each section were enumerated.

Measurement of the Production of mROS and Cellular Hydrogen Peroxide. BMMs were seeded onto six-well plates with each well containing 3×10^6 cells in 3 mL BMM media. Following overnight incubation, BMMs were infected with *S. Typhimurium* SL1344 (MOI 10) for 30 min. To measure mROS production, supernatant was aspirated and replenished with fresh prewarmed DMEM supplemented with 5 μ M MitoSOX Red superoxide indicator (M36008, Molecular Probes; Life Technologies) for 10 min at 37 °C. For the detection of cellular H₂O₂, cells were incubated in DMEM with 5 μ M CM-H₂DCFDA (M36008, Molecular Probes; Life Technologies), a chloromethyl derivative of H₂DCFDA, for 30 min at 37 °C. Cells were washed three times with prewarmed sterile PBS (Sigma) and collected using cell scrapers. Cells were pelleted by centrifugation (194 \times g, 5 min) and resuspended in 0.5 mL 2% (wt/vol) paraformaldehyde in MACS buffer (DPBS supplemented with 0.5% vol/vol FCS and 2 mM EDTA). The levels of mROS and H₂O₂ production were analyzed using the FACScan flow cytometer (BD Biosciences). The excitation and emission wavelengths used to detect MitoSOX staining were 510 and 580 nm, respectively. The excitation and emission wavelengths used to detect CM-H₂DCFDA staining were 495 and 519 nm, respectively. Ten thousand BMMs were analyzed using the FACScan flow cytometer for each repeat of the mROS and H₂O₂ experiment. The excitation and emission wavelengths used to detect CM-H₂DCFDA staining were 495 and 519 nm, respectively.

ELISA. Levels of mouse IL-1 β secreted into the supernatant were measured using the BD OptEIA Mouse IL-1 β set according to the manufacturer's instructions (BD Biosciences).

Statistical Analysis. Statistical significance between values from two groups was determined using unpaired Student *t* test, and values between three or more groups was determined using one- or two-way ANOVA with all values corrected using a multiple comparisons test. $P < 0.05$ is considered significant. Statistical analysis was performed using GraphPad Prism version 6 (GraphPad Software).

- Man SM, et al. (2014) Inflammasome activation causes dual recruitment of NLR4 and NLRP3 to the same macromolecular complex. *Proc Natl Acad Sci USA* 111(20):7403–7408.
- Guck J, et al. (2001) The optical stretcher: A novel laser tool to micromanipulate cells. *Biophys J* 81(2):767–784.
- Guck J, et al. (2005) Optical deformability as an inherent cell marker for testing malignant transformation and metastatic competence. *Biophys J* 88(5):3689–3698.
- Lautenschläger F, et al. (2009) The regulatory role of cell mechanics for migration of differentiating myeloid cells. *Proc Natl Acad Sci USA* 106(37):15696–15701.
- Guck J, Ananthakrishnan R, Moon TJ, Cunningham CC, Käs J (2000) Optical deformability of soft biological dielectrics. *Phys Rev Lett* 84(23):5451–5454.
- Boyd L, Chalut KJ, Guck J (2009) Interaction of Gaussian beam with near-spherical particle: An analytic-numerical approach for assessing scattering and stresses. *J Opt Soc Am A Opt Image Sci Vis* 26(8):1814–1826.
- Boyd L, Ekpenyong A, Whyte G, Guck J (2012) Comparison of stresses on homogeneous spheroids in the optical stretcher computed with geometrical optics and generalized Lorenz-Mie theory. *Appl Opt* 51(33):7934–7944.
- Chalut KJ, Ekpenyong AE, Clegg WL, Melhuish IC, Guck J (2012) Quantifying cellular differentiation by physical phenotype using digital holographic microscopy. *Integr Biol (Camb)* 4(3):280–284.
- Ekpenyong AE, et al. (2013) Bacterial infection of macrophages induces decrease in refractive index. *Journal of biophotonics* 6(5):393–397.
- Wottawah F, et al. (2005) Optical rheology of biological cells. *Phys Rev Lett* 94(9):098103.

